Accepted: 21 November 2023

DOI: 10.1002/lsm.23746

BASIC SCIENCE ARTICLE

Spectral effects and enhancement quantification in healthy human saliva with surface-enhanced Raman spectroscopy using silver nanopillar substrates

Esmat Zamani BEng[1,2] | Nassim Ksantini MSc[1,2] | Guillaume Sheehy MSc[1,2] | Katherine J. I. Ember PhD[1,2] | Bill Baloukas PhD[1] | Oleg Zabeida PhD[1] | Tran Trang BSc[1,2] | Myriam Mahfoud MEng[1,2] | Jolanta-Ewa Sapieha PhD[1] | Ludvik Martinu PhD[1] | Frédéric Leblond PhD[1,2]

[1]Department of Engineering Physics, Polytechnique Montreal, Montréal, Canada

[2]Centre de Recherche du Centre Hospitalier de l'Université de Montréal, Montreal, Canada

Correspondence
Frédéric Leblond, PhD, Department of Engineering Physics, Polytechnique Montreal, Montréal, Canada.
Email: frederic.leblond@polymtl.ca

Abstract

Objectives: Raman spectroscopy as a diagnostic tool for biofluid applications is limited by low inelastic scattering contributions compared to the fluorescence background from biomolecules. Surface-enhanced Raman spectroscopy (SERS) can increase Raman scattering signals, thereby offering the potential to reduce imaging times. We aimed to evaluate the enhancement related to the plasmonic effect and quantify the improvements in terms of spectral quality associated with SERS measurements in human saliva.

Methods: Dried human saliva was characterized using spontaneous Raman spectroscopy and SERS. A fabrication protocol was implemented leading to the production of silver (Ag) nanopillar substrates by glancing angle deposition. Two different imaging systems were used to interrogate saliva from 161 healthy donors: a custom single-point macroscopic system and a Raman micro-spectroscopy instrument. Quantitative metrics were established to compare spontaneous RS and SERS measurements: the Raman spectroscopy quality factor (QF), the photonic count rate (PR), the signal-to-background ratio (SBR).

Results: SERS measurements acquired with an excitation energy four times smaller than with spontaneous RS resulted in improved QF, PR values an order of magnitude larger and a SBR twice as large. The SERS enhancement reached 100×, depending on which Raman bands were considered.

Conclusions: Single-point measurement of dried saliva with silver nanopillars substrates led to reproducible SERS measurements, paving the way to real-time tools of diagnosis in human biofluids.

KEYWORDS

biofluids, metrology, microscopy, plasmonics, surface-enhanced Raman spectroscopy, tissue optics

INTRODUCTION

Human biofluids are commonly used in screening, therapeutic and diagnostic applications as they enable the direct measurement of circulating biomarkers related to a patient's health. Recently, as the COVID-19 pandemic unfolded, multiple emerging techniques for fast, label-free, non-invasive screening methods were developed.[1–7] However, given the urgency of the need to screen large numbers of people, more established techniques–including reverse transcription polymerase chain reaction (RT-PCR)–were widely used for viral detection in blood, nasopharyngeal swaps, but also in saliva.[8–10] Despite being generally highly sensitive, techniques such as RT-PCR are often time-intensive and require costly chemical reagents. Saliva has garnered interest as a biofluid for diagnostic applications,[10,11] as it is an easily obtainable biofluid due to the noninvasive nature of the sampling process.

Raman spectroscopy has been used for decades as a non-destructive tool for analysis of chemical, physical and biological analytes, and multiple research groups have explored spontaneous Raman spectroscopy (spontaneous RS) as a diagnostic method.[6,12–22] Raman spectroscopy, coupled with machine learning (ML) techniques, can detect biomolecular features associated with vibrational modes of bonds from lipids, nucleic acids, proteins, as well as specific amino acids.[12,13,23–27] Raman spectroscopy has been applied to biofluids for multiple detection purposes in dentistry,[28–31] forensics,[30–35] illicit drugs[30,31,36–38] and healthcare.[30,31,39,40]

Raman spectroscopy is an optical technique that uses a spectrometer to measure the inelastic scattering of light following sample illumination with a monochromatic laser source, usually in the near-infrared range to limit the impact of fluorescence from biomolecules. The method provides a non-destructive, and label-free molecular fingerprint that is intrinsic to the probed sample.[12] However, Raman spectroscopy is not without inconveniences. In healthcare and biomedical applications, the analysis of biomarkers lacks standardization in methodology and analysis, hindering commercialization and real-world use.[30,31] In addition, the low efficiency of Raman scattering coupled to the sensitivity and specificity required for biomedical diagnosis can necessitate high integration time and laser power, which can limit practical use in clinical applications.[41] For example, the laser power for an in vivo measurement should be limited to avoid tissue damages[42–44] and acquisition time must be short to fit into the clinical workflow, e.g., for surgical applications.[45–48]

Surface-enhanced Raman spectroscopy (SERS) leads to an inelastic scattering signal enhancement associated with an analyte adsorbed onto, or close to, a nanostructured surface. While the fundamental physics associated with the enhancement mechanism is still being studied, two mechanisms are known to be implicated: the electromagnetic mechanism (EM) and the chemical mechanism (CM).[41,49,50] The EM, considered to be the main contributor to the enhancement, relies on the generation of an intense localized electric field caused by the excitation of surface plasmon resonances from a roughened metallic surface (e.g., Au, Ag, and Cu). While signal enhancement magnitudes for SERS have been reported to be as high as 10^{10},[41] challenges remain to ensure reproducibility of the signal. This is due to the localized nature of the phenomenon[51,52] and the biomolecular interpretation of the resulting spectra. Interpretation can be made difficult because spectral bands of known biomolecular origin can shift, broaden or change due to a modification of the polarizability of the analytes adsorbed onto the surface.[41,51,52] This can limit the potential clinical use of SERS as a basis for the development of real-world biomedical applications. Clinical applications of SERS have been explored in oncology,[53–58] virology[7,59–61] and other diseases.[62,63] When used to study biofluids, SERS can identify molecular features of a specimen through the analysis of the resulting Raman spectrum (location, height, and width of peaks) as well as through functionalization of the plasmonic surfaces. Recently, our group demonstrated the use of label-free Raman micro-spectroscopy for saliva-based detection of COVID-19 infection in samples from a testing clinic.[6] Several studies have used spontaneous RS and SERS for biomedical diagnostics, without establishing a large baseline of the signature of healthy saliva.[6,30,31,54,64]

In this paper, we present SERS and spontaneous RS measurements from 161 dried saliva samples from healthy donors. The spectral datasets were acquired using two spectroscopic imaging systems based on specimen interrogation protocols optimized for saliva supernatant. One system was a commercial Raman micro-spectrometer that allowed microscopic sampling of dried droplets, while the other system allowed macroscopic interrogation of whole droplets. The macroscopic measurements were made using a custom single-point bench-top system specifically developed by our group for biofluid imaging applications. SERS measurements were compared with spontaneous Raman spectroscopy measurements of the same specimens to assess spectral signature variations and measurement reproducibility across saliva samples from a broad population of healthy donors. Silver nanopillar substrates were used for SERS measurements while spontaneous RS measurements were acquired from saliva deposited on flat aluminum microscope slides. The effect of the substrate on the Raman signal from human saliva was investigated by computing the signal enhancement factor of peaks with known biological origin. The assignments of these peaks are based on an artificial model saliva. This work was designed to benchmark the reproducibility and performance of a spontaneous and surface-enhanced Raman approach for real-time acquisition of biomolecular data from human saliva, as a methodology to enable rapid diagnosis in biofluids (e.g., saliva, blood, urine). The noninvasive nature and ease of collection of human saliva make it a good candidate for enabling rapid diagnosis, while also providing challenges for the screening of fluids with low concentrations of analytes (biomarkers).

MATERIALS AND METHODS

Sample collection

A total of 161 saliva samples from different individuals were collected at the Centre de Recherche du Centre Hospitalier de l'Université de Montréal (CRCHUM) from donors in compliance with the guidelines from the CHUM Research Ethics Board (project number: 20.133).

TABLE 1 Basic demographic characteristics of the saliva donors.

	# (%)
Total number of volunteers	**161**
Age range	
13–20	1 (0.62)
21–40	100 (62.11)
41–60	52 (32.3)
61–80	8 (4.97)
Sex	—
Female	56 (34.78)
Male	51 (31.68)
Prefer not to say	54 (33.54)

The collection window began at 8 a.m. and ended at 12 p.m. Before donating their saliva sample, volunteers were asked to complete a questionnaire disclosing medical factors such as sex at birth, age, medication, underlying diseases. Cohort characteristics extracted from the questionnaire were reported in Table 1 and Table 3 (Appendix A).

Each individual donor was instructed to remove any contaminant such as lip balm or lipstick with removal wipes (About Face Cleansing Wipes; Micronova Manufacturing Inc.) and then asked to rinse their mouth three times with bottled water. After 5–10 min of waiting, the donors were asked to spit in a 50 mL Falcon tube to collect a volume ranging from 1.5 to 10 mL of saliva. The samples were then stored in a refrigerator at 4°C before being processed in a biosafety containment level 2 (BSL2), in biosafety cabinets. Samples were pipetted and transferred to 1.5 mL microcentrifuge tubes and centrifuged at 4000 RPM for 30 min at 4°C. From the centrifuged samples, most of the supernatant was extracted into a single 1.8 mL cryotube, from which 40–500 μL were aliquoted in up to five 1.8 mL cryotubes. The residual supernatant bordering the pellet was discarded, while the pellet was conserved. The supernatant and the pellet samples were stored at −80°C.

Preparation of silver nanopillar substrates

The Ag nanopillar substrates used in the SERS measurements were prepared using the glancing angle deposition (GLAD) method using an electron-beam evaporation source installed in a Boxer Pro coater (Leybold Optics) at Polytechnique Montréal. This method has been described by Barranco et al. and Suzuki et al.[65,66] The deposition was carried out at room temperature and at a base pressure of 2×10^{-6} Torr, using 99.99% pure Ag pellets (K.J. Lesker). The substrates were prepared on Si <100> wafers and glass slides using a two-step process: (1) by first growing a thin 50 nm-thick Ag mirror at normal incidence (0°), (2) by tilting the Ag mirrors at an incidence angle of 85° during the deposition process. This resulted in Ag nanocolumns with an angle of ~65°, an average pillar length of 140 nm and average width of 60 nm (Figure 1B, Figure 2). The surface plasmon resonance of the resulting substrates are in the near ultraviolet.[67,68] The plasmon peak is sensitive to the polarization (*s*-polarized, *p*-polarized or a combination of both) of the excitation light. For a combination of *s* and *p* polarization, the plasmon peak is at 357 nm.[67,68] In this manuscript, we refer to these substrates as Ag GLAD substrates. Further illustration of the substrates, the spatial distribution of the substrate Raman response and the deposition chamber are available in Figures 6–8 (Appendix A).

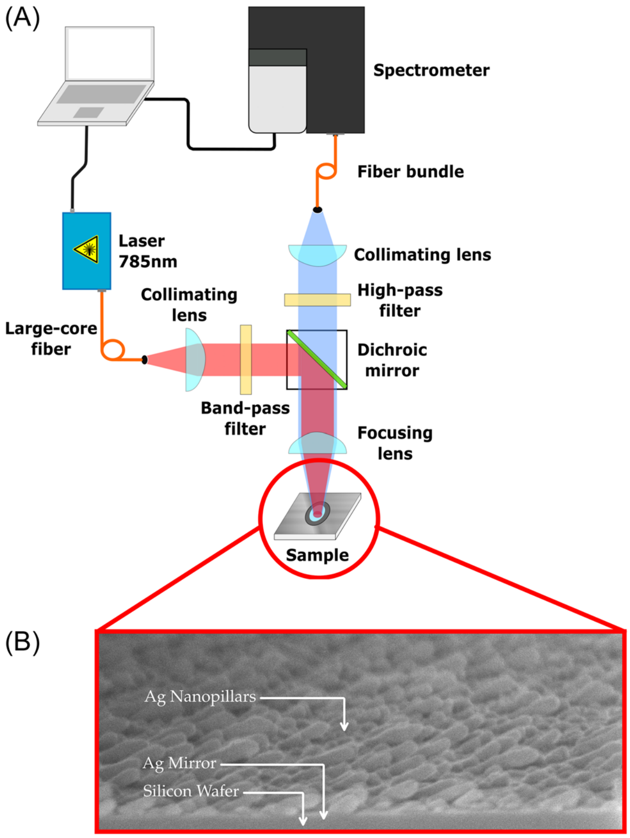

FIGURE 1 Schematic representation of the single-point imaging system and structure of the Ag GLAD substrates. (A) The system is in epi-illumination with a collection path formed from an excitation fiber, a collimating lens, a band-pass filter, a dichroic mirror and a focusing lens, which illuminates the sample in free space. The saliva sample is deposited onto an aluminum slide or a SERS substrate. The collection path includes a high-pass filter, a collimating lens and a fiber bundle which guides the scattered light to the spectrometer. The whole system is controlled by an Arduino microcontroller and an in-house custom acquisition interface built in MATLAB. (B) The cross-section of the substrate, obtained by scanning electron microscopy, shows an underlying structure where the nanopillars have an angle of ~65°, an average width of 60 nm and an average length of 140 nm.

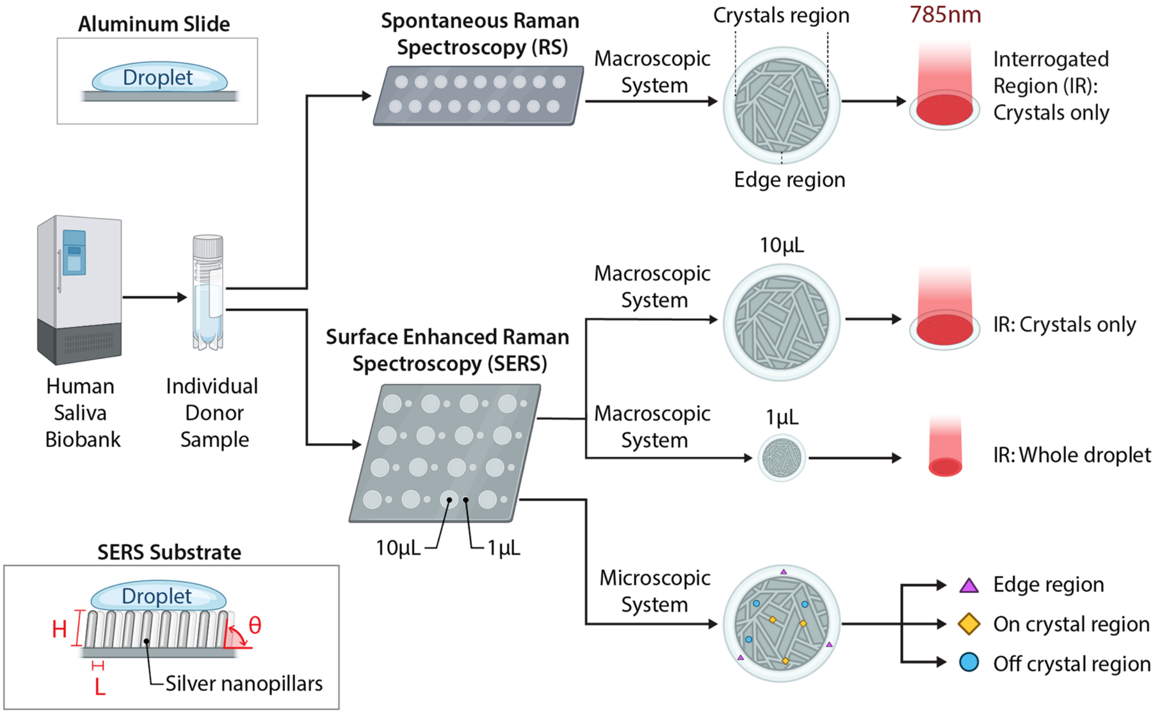

FIGURE 2 SERS and spontaneous RS saliva measurement workflow. Each saliva donor sample is collected from the saliva biobank, thawed for 30 min, deposited on a substrate, and dried for 45 min before proceeding with the relevant measurements. A 10 μL supernatant sample is then deposited on an aluminum slide for spontaneous RS in the center of the droplet (crystal region: *On crystal* measurement) with the single-point system. The 10 and 1 μL droplets from the same donor are deposited on a GLAD Ag substrate for SERS measurements with single-point system and the microscope system. The 10 μL droplet is imaged with the microscope using a protocol ensuring all morphological regions are interrogated: *Edge*, *On crystal* and *Off crystal*. Both the 10 and 1 μL droplets are interrogated with the single-point system, effectively resulting in crystal region (*On crystal* + *Off crystal*) and all-encompassing measurements, respectively. All-encompassing means that all morphological regions (*On crystal*, *Off crystal*, *Edge*) of the dried 1 μL droplet are interrogated with one single-point measurement.

Raman spectroscopy instrumentation

The samples in this study were imaged using two different systems: a commercial inVia™ confocal Raman microscope (Renishaw) in reflection mode and a custom-built single-point interrogation system.

The microscope was equipped with a motorized stage allowing multiple tiled brightfield images to be stitched together for a larger field of view (FOV) visualization. Measurements were carried out in the fingerprint region (602–1726 cm^{-1}) with a 50× long working distance objective (numerical aperture: 0.5, air immersion) and a 40 mW 785 nm laser with *in-line* mode (3 μm × 8 μm spot size). The spectrometer had a 1200 lines per millimeter reflection grating and a set of dielectric edge filters to filter the laser wavelength.

The single-point system was in epi-illumination mode and used a 785 nm laser source (Model IO785MM1500M4S; Innovative Photonic Solutions) with an output of 1.5 W and a spectral bandwidth <2 nm (Figure 1A). The other main constituent of the system was a spectrometer (HT model; EmVision) composed of a diffraction grating and a CCD camera (Newton 920; Oxford Instruments) resulting in a spectral resolution <8.7 cm^{-1}. An excitation fiber guided the light beam to a collimating lens and a band-pass filter (Semrock) before intersecting with a dichroic mirror reflecting light to a focusing lens onto the sample. The light re-emitted from the sample went through another focusing lens, the dichroic mirror, a high-pass filter (Semrock), a second collimating lens and a fiber bundle. The later was connected to the spectrometer and consisted of nine optical fibers with a core diameter of 300 μm and a numerical aperture of 0.22. The system also included a 3D motorized stage, a white light source and a brightfield camera. The system was controlled through an in-house custom acquisition MATLAB software (MathWorks) and a microcontroller (Arduino).

Measurement protocol

The saliva sample preparation and spectroscopic interrogation workflow is shown in Figure 2. All samples were thawed at room temperature for 30 min and vortexed during 40 s. Up to five 10 μL droplets of saliva supernatant were pipetted and deposited onto an aluminum slide in preparation for the spontaneous RS measurements, totaling 796 droplets across 161 donor samples. For each donor sample, two droplets –one of

1 μL and one of 10 μL–were also deposited onto an Ag GLAD substrate for the SERS measurements. All droplets were allowed to dry for 45 min.

Raman micro-spectroscopy was used to acquire spectral data from three distinct morphological regions, for each 10 μL droplet. Those regions consisted of the so-called *coffee ring* at the edge of dried samples (henceforth labeled *Edge*), directly on the crystals of the crystallized region (*On crystal*) and next to the crystals, in the vicinity of the *On crystal* measurements (*Off crystal*). Measurements within each region (*Edge*, *On crystal*, *Off crystal*) consisted of 5-10 points acquired randomly using the map functionality of the Wire 4.4 software (Renishaw, UK), that were then averaged. The laser power was set at 50% of its full power and the acquisition time ranged from 0.1 to 1 ms for the *On crystal* and *Off crystal* regions, and the time ranged from 0.25 to 2 s for the *Edge* region. Acquisition time was modulated such that 60-70% of the sensor dynamic range was utilized. Further details relating to the spectral data acquisition workflow are shown in Figure 9 (Appendix A).

Single-point spontaneous Raman spectroscopy measurements were acquired from the 10 μL and 1 μL droplets. The 10 μL droplet measurement was taken from the center of the sample with a laser power of 1400 mW and an acquisition time ranging from 5 to 200 ms, with a spot size of 0.5 mm^2. This allowed simultaneous interrogation of both the *On crystal* and *Off crystal* regions. The 1 μL droplet measurements were done using a larger core excitation fiber (1500 μm instead of 300 μm), resulting in an excitation spot size of 3.14 mm^2, effectively probing all morphological regions (*On crystal*, *Off crystal*, *Edge*) with a single measurement. For these measurements, the laser power was 1000 mW and the acquisition time ranged from 20 to 500 ms. Each measurement consisted of 20–500 spectra acquired at the same location that were averaged to increase the signal-to-noise ratio (SNR).

Spectral data preprocessing

All spectra acquired were processed using standard methods to isolate and display the inelastic scattering component of the detected spectral fingerprint.[69,70] Briefly, the following steps were applied: (1) cosmic rays were removed with a custom first derivative-based algorithm; (2) x axis was calibrated with a reference Raman specimen (Renishaw microscope: crystalline silicon; single-point system: acetaminophen), (3) y axis was calibrated for the single-point system with a NIST Raman standard, (4) the intensity of each individual spectrum was normalized by time and power; (5) N repeat measurements (i.e., accumulations) for each sample were averaged; (6) background contributions (e.g., autofluorescence) were removed using the *Bubblefill* algorithm using a minimum bubble window of size 40; (7) measurements were smoothed with a Savitzky-Golay filter of order 3 and a window size of 11; (8) a standard normal variate (SNV) normalization was applied.

Spectral quality metrics

Quantitative metrics were defined to compare the different types of measurements made, allowing a direct comparison between spontaneous RS and SERS measurements. Those metrics are: (1) the photonic count rate (PR), (2) the signal-to-background ratio (SBR), (3) the spectral quality factor (QF) and the SERS enhancement factor (EF).

The photonic count rate consists of the overall detected light intensity, normalized with the laser power, the integration time per measurement, and the number of accumulations. The SBR metric is defined as the ratio between the detected inelastic scattering over the background signal which is mostly associated with autofluorescence from saliva biomolecules. The inelastic scattering component of the signal is the integral under-the-curve of the actual Raman spectrum (before Savitzky-Golay filtering and SNV normalization), and the background value consists of the integral under-the-curve of the residual signal component from the application of the *BubbleFill* algorithm. These two metrics (PR and SBR) are important in comparing spontaneous RS and SERS measurements because plasmon-induced enhancement does not only impact Raman scattering but also fluorescence, resulting in surface-enhanced fluorescence (SEF).[41,50]

The QF is defined as the average signed squared intensity (ASSI) of the SNV-normalized Raman spectrum[69]:

$$QF := \frac{1}{n}\sum_{i=1}^{n}\text{sgn}\left(r_i^{\star}\right)\cdot r_i^{\star 2}, \tag{1}$$

where $r_i^{\star}$ is one spectral component (i runs from 1 to the total number of spectral bins n) and $\text{sgn}(r_i^{\star})$ is the sign function of $r_i^{\star}$, which is either -1 or 1. Applying this metric to a SNV-normalized Raman spectrum returns a value with a maximum of 1. A spectrum dominated by stochastic noise will typically return a low QF-value close to 0, while a high-quality spectrum returns a value closer to 1. The PR, SBR and QF were computed for all spontaneous RS and SERS measurements to show statistical distributions across all saliva samples.

In the SERS literature, the enhancement factor (EF) is defined as the ratio of the intensity of a spectral band using SERS relative to its equivalent measured without the presence of a nanostructured substrate using spontaneous RS. The EF is usually computed based on the coupling of a specific analyte (e.g., rhodamine) with a nanostructured substrate, and includes a normalization factor accounting for the actual concentration of the analyte.[71] For a specific Raman saliva band, the EF is the ratio of the area under the curve for SERS and spontaneous RS measurements. To compute the EF, all spectra are normalized with power (*P*), integration time (*t*) and number of accumulations (*N*) to ensure they can be compared to one another on an equal footing. To account from potential band broadening associated with the plasmonic effect, the intensity for each band is computed from the full width at half maximum (FWHM).[51]

RESULTS

Comparison between macroscopic and microscopic measurements

To determine the reproducibility of the SERS measurements, the SERS measurements of saliva, as described in the Methods section, were compared from a microscopic scale (Renishaw InVia Raman microscope) to a macroscopic scale (single-point system).

Figure 3A show the average SNV normalized spectra for the 10 μL droplet measurements, along with the inter-specimen standard deviation for each spectral bin. The spectra shown were those acquired with the single-point system for spontaneous RS and SERS, as well as the SERS spectra acquired with the microscope. The latter were computed by averaging all spectra acquired from the *On crystal* and *Off crystal* regions. Common Raman-active biomolecular peaks could be detected on the average spectrum from all systems, for both spontaneous and SERS measurements (Figure 3B). These included vibrational bonds at 731, 924, 1003, 1045, 1203 and 1449 cm^{-1}, for which a tentative biomolecular assignment is shown in Table 2 (Appendix A) based on a model saliva. This was made from mixing pure biomolecules and has been used in other studies including from our group.[6,72–74]

Figure 3A also presents the inelastic scattering response (single-point RS) of the Ag GLAD substrate after SNV normalization. By comparing the scale of all visually distinguishable bands (shown with the black curve) in the substrate versus the saliva measurements (main peaks, highlighted in dashed black boxes), it is apparent that the saliva signals are not dominated by Raman peaks from the Ag GLAD substrate. Furthermore, the width and position of the substrate peaks do not correlate directly with the main biomolecular saliva peaks from Table 2. Inspection of the six substrate bands in Figure 3A (696, 960, 1066, 1331, 1479, and 1606 cm^{-1}) further reveals that there is only a partial overlap of the Raman response of the SERS substrate with the saliva signal, except for the 1331 cm^{-1} peak where saliva signature detectability could be compromised (Figure 8) (Appendix A).

Visual inspection of the spectra in Figure 3A provides evidence that the combination of an Ag GLAD substrate with dried human saliva yields biomolecular information that is reproducible across specimens from different donors and for different spatial scales (macroscopic *vs.* microscopic). Moreover, the SERS signatures are comparable to the spontaneous Raman spectroscopy signatures, with the SERS measurement typically resulting in low levels of distortion, broadening and band shifting. One exception is the band at 1045 cm^{-1}, which is slightly shifted to 1048 cm^{-1}, as well as the emergence of a band at 1032 cm^{-1} detected on the SERS measurements, but not for the spontaneous RS measurements. Additionally, subtle discrepancies are seen in the six bands highlighted in Figure 3A, such as the relative intensities of the bands and the band widths. The widths of all highlighted bands are narrower on the microscope system relative to the same bands on the single-point system and the relative intensities are lower.

Surface enhancement effect on dried saliva

To evaluate the surface enhancement effect of dried saliva, single-point SERS 10 μL and single-point spontaneous RS 10 μL datasets were processed. The objective was to quantitatively compare them in terms of the quality factor (QF), photon count rate (PR), signal to background ratio (SBR) and enhancement factor (EF) metrics. The SERS measurements performed using the 1 μL droplets are not shown. They generally led to spectroscopic signals with reduced overall quality relative to the SERS μL measurements, as quantitatively assessed based on the PR, SBR and QF metrics. Furthermore, the EF factor could not be computed for these measurements since no equivalent all-encompassing spontaneous RS measurement was made on 1 μL droplets, due to limited volume of saliva available for each donor. Each data point is normalized by the acquisition parameters, which corresponds to the product of laser power (*P*), the integration time (*t*) and the number of accumulations (*N*). The product of these parameters represents the total energy (in Joules) deposited to the sample. The deposited energy ($P \times N \times t$) of SERS measurements was–on average–almost four times less when compared to spontaneous RS measurements.

Figure 4 presents the distribution of these metrics (*y* axis) as a function of the droplet number (*x* axis). Figure 4A shows the QF distribution for the spontaneous RS measurements while Figure 4B shows the same metric computed for the SERS measurements. The median QF value is highlighted on the figures, as well as a QF threshold at 0.5. This specific threshold is shown because past studies from our group demonstrated, mostly in biological tissues, that QF values larger than 0.5 are usually associated with Raman spectra of high quality, typically showing strong, biologically relevant Raman bands (e.g., amide bands in protein-rich tissue).[20] Overall, the QF is higher for

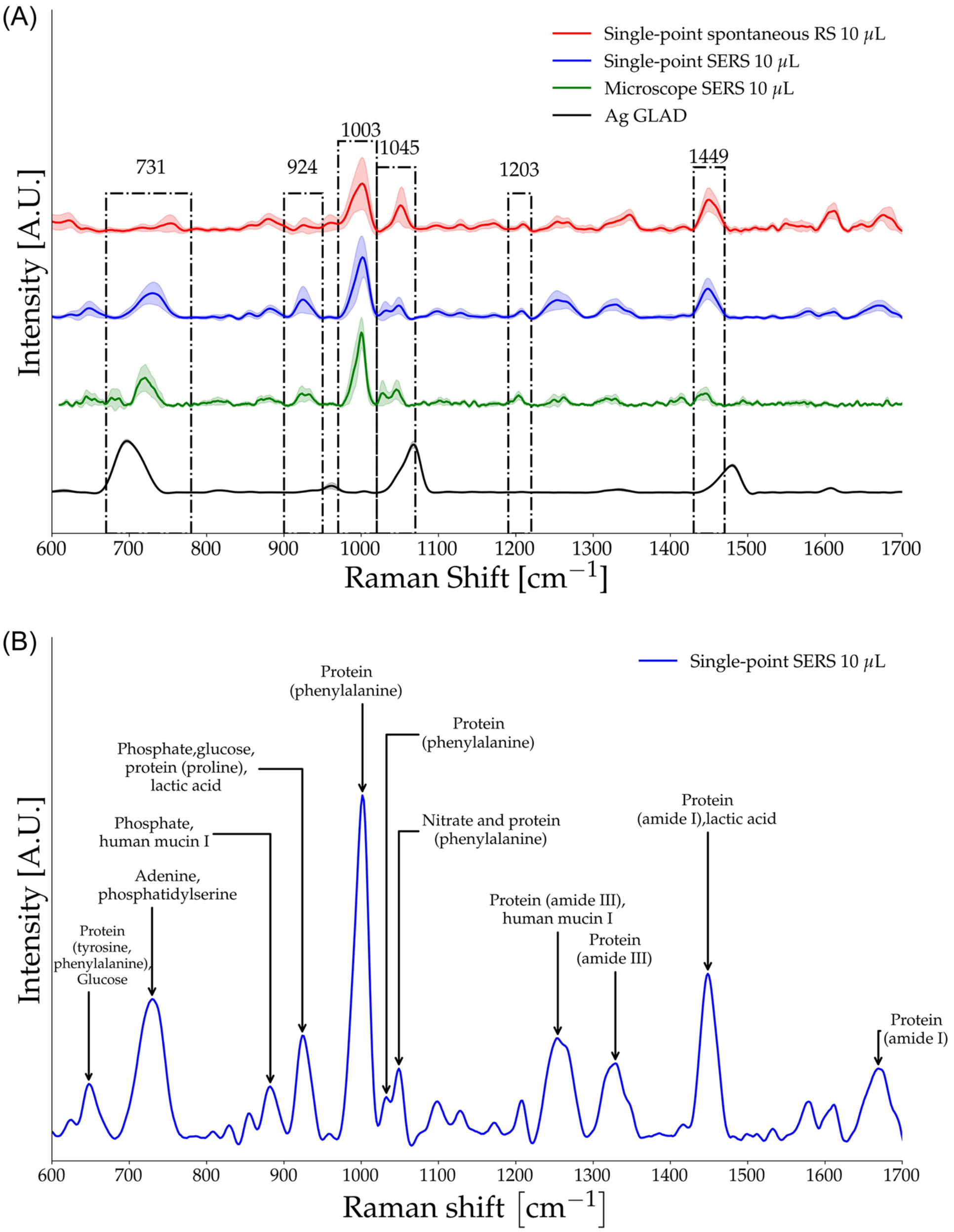

FIGURE 3 Comparison of the SERS and spontaneous RS signals from the crystal region of dried saliva droplets acquired with different instruments. (A) Average SNV-normalized spectra with the standard deviation from SERS and spontaneous RS measurements, using the single-point system and a Renishaw InVia microscope, with six bands of known biomolecular origin highlighted (731, 924, 1003, 1045, 1203, and 1449 cm^{-1}). The inelastic scattering response of the Ag GLAD substrate is shown. (B) Tentative biomolecular band assignment of the average SERS saliva spectrum from the crystal region, based on the measurement of the Raman spectra from an artificial model saliva and its subcomponents.

the SERS spectra, with a median of 0.69 compared to a median of 0.61 for the spontaneous RS measurements. Further, 94% of the SERS spectra have a QF value higher than 0.5, compared to 70% for the spontaneous RS spectra.

Figure 4C shows the PR distribution for the spontaneous RS measurements while Figure 4D shows the same metric computed from the SERS measurements. The dotted line represents the average PR value for each distribution. On average, the sum of Raman and autofluorescence contributions is approximately an order of magnitude higher ($\text{PR} = 4.1 \times 10^3$) for SERS measurement when compared to spontaneous RS measurements ($\text{PR} = 5.3 \times 10^2$). This was achieved despite the deposited energy being approximately four times higher for spontaneous RS measurements.

Figure 4D shows the SBR distribution for the spontaneous RS measurements while Figure 4E shows the same metric computed from the SERS measurements. The dotted line represents the average SBR value for each distribution. Factoring the acquisition parameters, on average, the SERS measurement SBR (SBR =

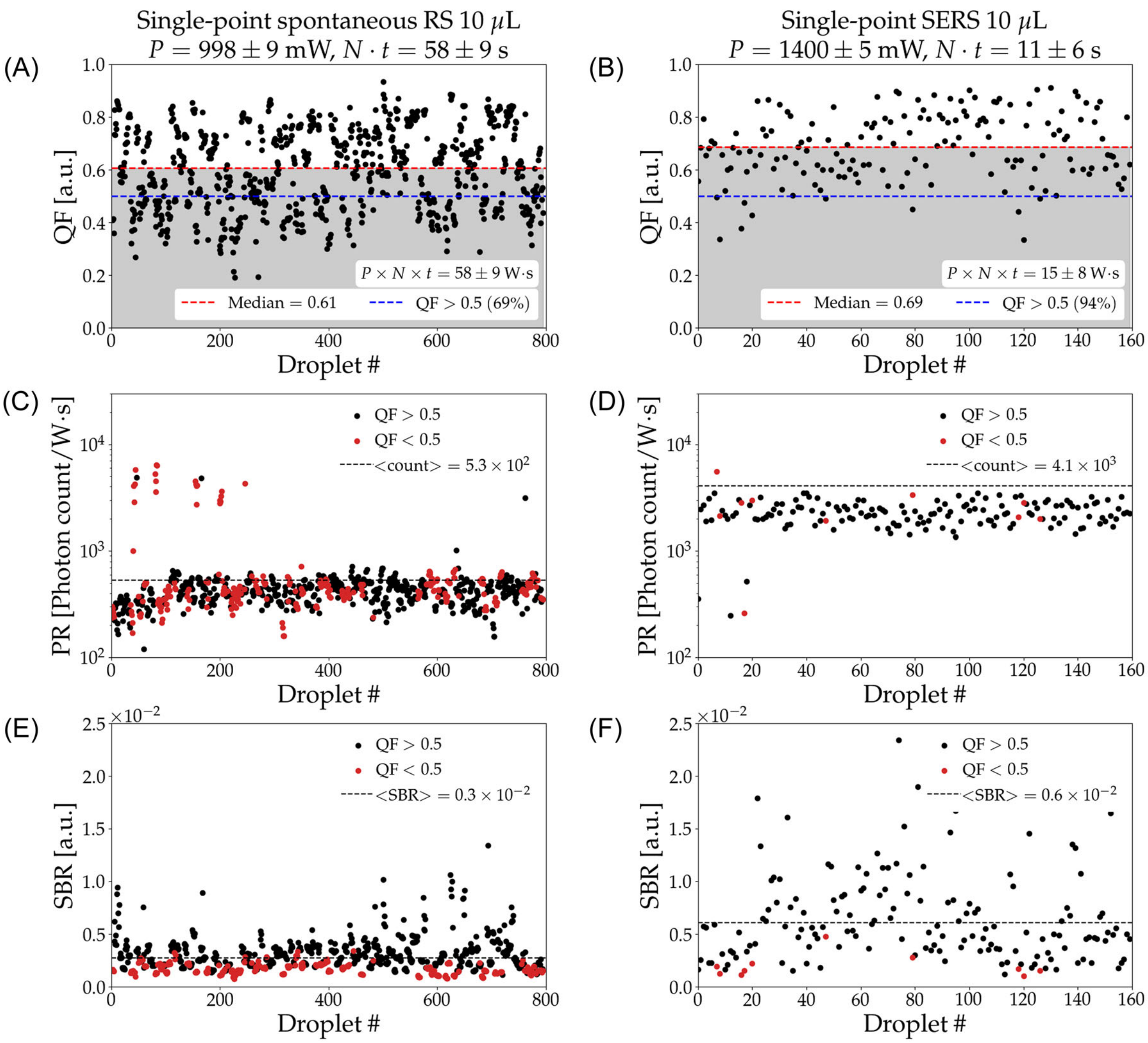

FIGURE 4 Spectral quality metrics computed for the SERS and spontaneous RS datasets acquired with the single-point system for a 10 µL saliva droplet. Quality Factor (QF) with dotted lines associated with the median and a QF cutoff at 0.5 for: (A) spontaneous RS spectra, (B) SERS spectra; Photonic count rate (PR) with dotted line associated with the average for: (C) spontaneous RS spectra, (D) SERS spectra; Signal-to-background ratio (SBR) with a dotted line associated with the average for: (A) spontaneous RS spectra, (B) SERS spectra. For the PR and SBR distributions, measurements colored black are associated with $QF > 0.5$, while those that are colored red are associated with $QF < 0.5$.

0.6×10^{-2}) was twice that of the spontaneous RS measurements ($SBR = 0.3 \times 10^{-2}$).

The EF was computed from the SERS and the spontaneous RS measurements. The averaged spectroscopic signal for each data set was computed from raw signals normalized in terms of P, t and N. All spectral pre-processing steps were applied except SNV normalization, resulting in the average SERS and spontaneous RS spectra in Figure 5A. The EF was then computed for each spectral bin with results shown Figure 5B in the form of a histogram. Enhancement factors ranged from 4× to values larger than 100 for some bands.

These results indicate that the Ag GLAD substrate coupled with dried human saliva generates a net enhancement in Raman scattering. Hence, Figure 4 and Figure 5 indicate that on average, SERS saliva measurements lead to larger QF, PR and SBR values.

DISCUSSION

The study first demonstrated that three independent measurement types, using two different imaging systems, led to consistent and reproducible dried saliva Raman spectroscopy signatures. The objective was to assess if a significant inelastic scattering enhancement, driven by the plasmonic effect, could be induced leading to reduced imaging times when compared to spontaneous Raman spectroscopy methods. Another aim was to determine whether macroscopic SERS measurements in human saliva could be realized in a manner that was reproducible within a large population of 161 human donors. Consistency was assessed based on the presence of ubiquitous biomolecular peaks with known origin terms of vibrational bonds based on saliva models. In that respect, the results demonstrated two things: first, that measurements made with a Raman

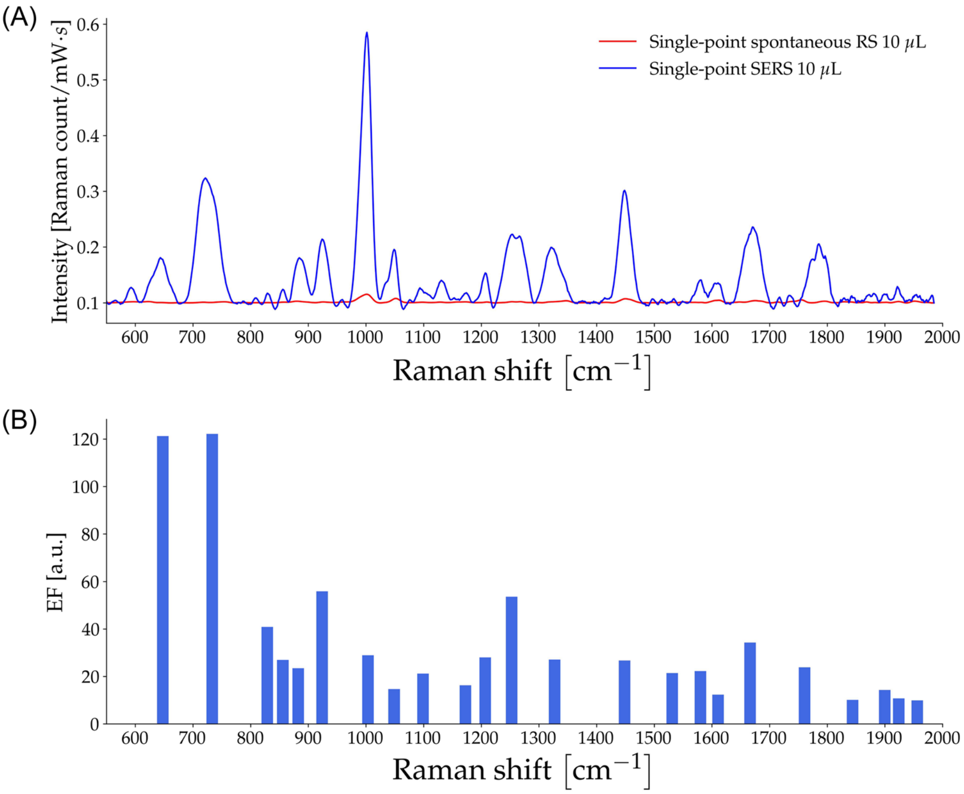

FIGURE 5 Enhancement computed from the SERS and spontaneous RS datasets: (A) Average normalized Raman response of the single-point measurements, (B) enhancement factor (EF) computed from the spectra in (A).

micro-spectrometer and a custom single point instrument were consistent; secondly, that SERS and spontaneous RS measurements resulted in similar Raman spectral fingerprints. This is important because an often-cited problem with SERS is the variability of the spectroscopic signals due to the local nature of the surface enhancement mechanism and the methodological approach selected to probe analytes.[51,52] Similar to SERS, other Raman spectroscopy techniques aim to enhance Raman scattering and reduce required laser power and acquisition times. Some of these approaches are based on nonlinear light-matter interaction phenomena, including stimulated Raman spectroscopy (SRS), coherent stimulated Raman spectroscopy (CSRS) and coherent anti-Stokes Raman spectroscopy (CARS).[75] Unlike SERS, the nonlinear techniques (CARS, SRS, and CSRS) require more costly imaging systems and are usually limited to select spectral wavenumber ranges of detection, thus limiting the molecular information collected from spectroscopic measurements.[12] However, added complexity to nonlinear imaging systems can overcome those challenges.[76–78]

The results presented here showed that drying the biofluid analytes on surfaces (aluminum slides for spontaneous RS, sliver nanopillars for SERS) led to sufficiently homogenous distributions of analytes to achieve consistent inelastic scattering signals independent of spatial sampling scale. This is hypothesized to be in large part due to the high quality of the silver nanopillar substrates that were produced, using custom protocols optimized to be highly repeatable and to minimize geometrical variations across the imaging domain (e.g., nanopillar height, width, and density). This ensured all measurement, either at microscopic or macroscopic scales, effectively averaged local variability of the substrate-analyte couplings in a manner that was repeatable across samples.[41,51,52] Tentative band assignment was based on an artificial saliva model. From the band assignment, the enhancement of the Raman bands of the saliva generated low level of band shifting, distortion and broadening. Band assignment for a SERS spectrum is a complex subject. Generally, numerical approaches such as Density Functional Theory (DTF) can be used to compute the vibrational degree of freedom of an analyte and deduce the specific mode resulting in a Raman band in a simplified configuration. The same approach can be applied to SERS. While the DFT simulations do not reproduce exactly the empirical SERS bands (charge transfer effects are not well described by DFT), they tend to give an idea of the driving Raman response.[49,50] Subsequently, quantitative metrics were established to provide a robust comparison between spontaneous RS and SERS measurements. In summary, when compared to spontaneous RS the SERS measurements acquired with a sample excitation energy four times smaller resulted in improved Raman spectrum QF, PR values an order of magnitude larger and a SBR twice as large.

This resulted in enhancement factors, assessed based on the EF metric, ranging from approximately 4× to more than 100×, depending on which Raman bands were considered. The enhancement factor achieved with saliva is more modest compared to the achievable potential of the Ag GLAD substrates. The enhancement factor of Ag GLAD substrates is dependent upon length and width of the pillars. With a length of 500 nm, those substrates can reach a local enhancement factor ranging 10^5–10^8 for measurements on trans-1,2-bis(4-pyridyl)ethene (BPE).[67,68] With a range of length of 140-200 nm, the EF diminishes to reach 10^3–10^4.[67,68] The substrate in this study has an average length of 140 nm, meaning the enhancement achievement 10^2 is, in principle, an order of magnitude lower than what could have been expected. In the future, multiple parameters could be tuned to maximize the EF, such as longer deposition time to increase the nanopillars length and width or the wavelength of excitation.

CONCLUSION

We demonstrated that the coupling between the silver nanopillars substrates and dried saliva supernatant resulted on average in a net enhancement gain relative to a spontaneous Raman measurement, on the morphological region encompassing the crystals. The macroscopic single-point imaging approach correlated with most SERS bands in the fingerprint region relative to a commercial Raman microscope. This suggests that the robustness of the microscope system can be replicated with a single-point system without the expensive time cost of completing a measurement across the different morphological zone of a dried droplet. The versatility of this multimodal methodology is multifold: it can provide label-free (spontaneous RS) or targeted (functionalized SERS) biomolecular information for a wide range of diseases, it can be applied to different biofluids (e.g., saliva, blood, urine) and finally enable real-time diagnostics on biofluids assisted with machine learning methodologies, reducing the time burden to achieve scale in building a substantial sample data set.

ACKNOWLEDGMENTS

The authors acknowledge funding from the Canada First Research Excellence Fund (TransMedTech Institute, IVADO), the Natural Sciences and Engineering Research Council of Canada (Alliance and Discovery grant programs) and the Canada Foundation for Innovation (Exceptional Opportunities Fund program).

CONFLICT OF INTEREST STATEMENT

The authors declare no conflict of interest.

ORCID

Esmat Zamani http://orcid.org/0000-0001-7280-1059

REFERENCES

1. Adi W, Biswas D, Shelef MA, Yesilkoy F. Multiplexed COVID-19 antibody quantification from human sera using label-free nanoplasmonic biosensors. Biomed Opt Express. 2022;13(4):2130. https://doi.org/10.1364/BOE.454919
2. Goswami N, He YR, Deng YH, Oh C, Sobh N, Valera E, et al. Label-free SARS-CoV-2 detection and classification using phase imaging with computational specificity. Light Sci Appl. 2021;10(1):176. https://doi.org/10.1038/s41377-021-00620-8
3. Khayamian MA, Parizi MS, Ghaderinia M, Abadijoo H, Vanaei S, Simaee H, et al. A label-free graphene-based impedimetric biosensor for real-time tracing of the cytokine storm in blood serum; suitable for screening COVID-19 patients. RSC Adv. 2021;11(55):34503–15. https://doi.org/10.1039/D1RA04298J
4. Roberts A, Mahari S, Shahdeo D, Gandhi S. Label-free detection of SARS-CoV-2 spike S1 antigen triggered by electroactive gold nanoparticles on antibody coated fluorine-doped tin oxide (FTO) electrode. Anal Chim Acta. 2021;1188:339207. https://doi.org/10.1016/j.aca.2021.339207
5. van Kooten XF, Rozevsky Y, Marom Y, Ben Sadeh E, Meller A. Purely electrical SARS-CoV-2 sensing based on single-molecule counting. Nanoscale. 2022;14(13):4977–86. https://doi.org/10.1039/D1NR07787B
6. Ember K, Daoust F, Mahfoud M, Dallaire F, Ahmad EZ, Tran T, et al. Saliva-based detection of COVID-19 infection in a real-world setting using reagent-free Raman spectroscopy and machine learning. J Biomed Opt. 2022;27(02):025002. https://doi.org/10.1117/1.JBO.27.2.025002
7. Carlomagno C. COVID-19 salivary Raman fingerprint: innovative approach for the detection of current and past SARS-CoV-2 infections. Sci Rep. 2021;11(1):4943. https://doi.org/10.1038/s41598-021-84565-3
8. Maxim LD, Niebo R, Utell MJ. Screening tests: a review with examples. Inhal Toxicol. 2014;26(13):811–28. https://doi.org/10.3109/08958378.2014.955932
9. Moeller KE, Lee KC, Kissack JC. Urine drug screening: practical guide for clinicians. Mayo Clin Proc. 2008;83(1):66–76. https://doi.org/10.4065/83.1.66
10. Mortimer PP, Parry JV. The use of saliva for viral diagnosis and screening. Epidemiol Infect. 1988;101(2):197–201. https://doi.org/10.1017/S0950268800054108
11. Lukose J, M. SP, N. M, Barik AK, Pai KM, Unnikrishnan VK, et al. Photonics of human saliva: potential optical methods for the screening of abnormal health conditions and infections. Biophys Rev. 2021;13(3):359–85. https://doi.org/10.1007/s12551-021-00807-8
12. Shipp DW, Sinjab F, Notingher I. Raman spectroscopy: techniques and applications in the life sciences. Adv Opt Photonics. 2017;9(2):315. https://doi.org/10.1364/AOP.9.000315
13. Bielecki C, Bocklitz TW, Schmitt M, Krafft C, Marquardt C, Gharbi A, et al. Classification of inflammatory bowel diseases by means of Raman spectroscopic imaging of epithelium cells. J Biomed Opt. 2012;17(7):0760301. https://doi.org/10.1117/1.JBO.17.7.076030
14. Bouzy P, Lyburn ID, Pinder SE, Scott R, Mansfield J, Moger J, et al. Exploration of utility of combined optical photothermal infrared and Raman imaging for investigating the chemical composition of microcalcifications in breast cancer. Anal Methods. 2023;15(13):1620–30. https://doi.org/10.1039/D2AY01197B
15. Ghita A, Matousek P, Stone N. High sensitivity non-invasive detection of calcifications deep inside biological tissue using transmission Raman spectroscopy. J Biophoton. 2018;11(1):e201600260. https://doi.org/10.1002/jbio.201600260
16. Kirchberger-Tolstik T, Pradhan P, Vieth M, Grunert P, Popp J, Bocklitz TW, et al. Towards an interpretable classifier for characterization of endoscopic mayo scores in ulcerative colitis using Raman spectroscopy. Anal Chem. 2020;92(20):13776–84. https://doi.org/10.1021/acs.analchem.0c02163

17. Kirchberger-Tolstik T, Ryabchykov O, Bocklitz T, Dirsch O, Settmacher U, Popp J, et al. Nondestructive molecular imaging by Raman spectroscopy *vs.* marker detection by MALDI IMS for an early diagnosis of HCC. Analyst (Lond). 2021;146(4):1239–52. https://doi.org/10.1039/D0AN01555E
18. Almond LM, Hutchings J, Shepherd N, Barr H, Stone N, Kendall C. Raman spectroscopy: a potential tool for early objective diagnosis of neoplasia in the oesophagus. J Biophoton. 2011;4(10):685–95. https://doi.org/10.1002/jbio.201100041
19. Nicolson F, Kircher MF, Stone N, Matousek P. Spatially offset Raman spectroscopy for biomedical applications. Chem Soc Rev. 2021;50(1):556–68. https://doi.org/10.1039/D0CS00855A
20. David S, Trang T, Dallaire F, et al. In situ Raman spectroscopy and machine learning unveil biomolecular alterations in breast cancer. J Biomed Opt. 2023;28(3):036009. https://doi.org/10.1117/1.JBO.28.3.036009
21. Picot F, Shams R, Dallaire F, Sheehy G, Trang T, Grajales D, et al. Image-guided Raman spectroscopy navigation system to improve transperineal prostate cancer detection. Part 1: Raman spectroscopy fiber-optics system and in situ tissue characterization. J Biomed Opt. 2022;27(09):095003. https://doi.org/10.1117/1.JBO.27.9.095003
22. Grajales D, Picot F, Shams R, Dallaire F, Sheehy G, Alley S, et al. Image-guided Raman spectroscopy navigation system to improve transperineal prostate cancer detection. Part 2: in-vivo tumor-targeting using a classification model combining spectral and MRI-radiomics features. J Biomed Opt. 2022;27(09):095004. https://doi.org/10.1117/1.JBO.27.9.095004
23. DePaoli D, Lemoine É, Ember K, Parent M, Prud'homme M, Cantin L, et al. Rise of Raman spectroscopy in neurosurgery: a review. J Biomed Opt. 2020;25(05):1. https://doi.org/10.1117/1.JBO.25.5.050901
24. Jermyn M, Mok K, Mercier J, Desroches J, Pichette J, Saint-Arnaud K, et al. Intraoperative brain cancer detection with Raman spectroscopy in humans. Sci Transl Med. 2015;7(274):274ra19. https://doi.org/10.1126/scitranslmed.aaa2384
25. Jermyn M, Mercier J, Aubertin K, Desroches J, Urmey K, Karamchandiani J, et al. Highly accurate detection of cancer in situ with intraoperative, label-free, multimodal optical spectroscopy. Cancer Res. 2017;77(14):3942–50. https://doi.org/10.1158/0008-5472.CAN-17-0668
26. Daoust F, Nguyen T, Orsini P, Bismuth J, de Denus-Baillargeon MM, Veilleux I, et al. Handheld macroscopic Raman spectroscopy imaging instrument for machine-learning-based molecular tissue margins characterization. J Biomed Opt. 2021;26(02):022911. https://doi.org/10.1117/1.JBO.26.2.022911
27. Pence IJ, Beaulieu DB, Horst SN, Bi X, Herline AJ, Schwartz DA, et al. Clinical characterization of in vivo inflammatory bowel disease with Raman spectroscopy. Biomed Opt Express. 2017;8(2):524. https://doi.org/10.1364/BOE.8.000524
28. Gonchukov S, Sukhinina A, Bakhmutov D, Minaeva S. Raman spectroscopy of saliva as a perspective method for periodontitis diagnostics. Laser Phys Lett. 2012;9(1):73–7. https://doi.org/10.1002/lapl.201110095
29. Gonchukov S, Sukhinina A, Bakhmutov D, Biryukova T, Tsvetkov M, Bagratashvily V. Periodontitis diagnostics using resonance Raman spectroscopy on saliva. Laser Phys Lett. 2013;10(7):075610. https://doi.org/10.1088/1612-2011/10/7/075610
30. Buchan E, Hardy M, Gomes PC, Kelleher L, Chu HOM, Oppenheimer PG. Emerging Raman spectroscopy and saliva-based diagnostics: from challenges to applications. Appl Spectrosc Rev. 2022:1–38. https://doi.org/10.1080/05704928.2022.2130351
31. Hardy M, Kelleher L, de Carvalho Gomes P, Buchan E, Chu HOM, Goldberg Oppenheimer P. Methods in Raman spectroscopy for saliva studies–a review. Appl Spectrosc Rev. 2022;57(3):177–233. https://doi.org/10.1080/05704928.2021.1969944
32. Muro CK, Doty KC, de Souza Fernandes L, Lednev IK. Forensic body fluid identification and differentiation by Raman spectroscopy. Forensic Chem. 2016;1:31–8. https://doi.org/10.1016/j.forc.2016.06.003
33. Sikirzhytski V, Virkler K, Lednev IK. Discriminant analysis of Raman spectra for body fluid identification for forensic purposes. Sensors. 2010;10(4):2869–84. https://doi.org/10.3390/s100402869
34. Sikirzhytski V, Sikirzhytskaya A, Lednev IK. Multidimensional Raman spectroscopic signatures as a tool for forensic identification of body fluid traces: a review. Appl Spectrosc. 2011;65(11):1223–32. https://doi.org/10.1366/11-06455
35. Sikirzhytski V, Sikirzhytskaya A, Lednev IK. Advanced statistical analysis of Raman spectroscopic data for the identification of body fluid traces: semen and blood mixtures. Forensic Sci Int. 2012;222(1–3):259–65. https://doi.org/10.1016/j.forsciint.2012.07.002
36. Hodges CM, Hendra PJ, Willis HA, Farley T. Fourier transform Raman spectroscopy of illicit drugs. J Raman Spectrosc. 1989;20(11):745–9. https://doi.org/10.1002/jrs.1250201108
37. Ryder AG, O'Connor GM, Glynn TJ. Identifications and quantitative measurements of narcotics in solid mixtures using near-IR Raman spectroscopy and multivariate analysis. J Forensic Sci. 1999;44(5):12031J. https://doi.org/10.1520/JFS12031J
38. Jones LE, Stewart A, Peters KL, McNaul M, Speers SJ, Fletcher NC, et al. Infrared and Raman screening of seized novel psychoactive substances: a large scale study of >200 samples. Analyst (Lond). 2016;141(3):902–9. https://doi.org/10.1039/C5AN02326B
39. Maitra I, Morais CLM, Lima KMG, Ashton KM, Date RS, Martin FL. Raman spectral discrimination in human liquid biopsies of oesophageal transformation to adenocarcinoma. J Biophotonics. 2020;13(3):e201960132. https://doi.org/10.1002/jbio.201960132
40. Carlomagno C, Banfi PI, Gualerzi A, Picciolini S, Volpato E, Meloni M, et al. Human salivary Raman fingerprint as biomarker for the diagnosis of amyotrophic lateral sclerosis. Sci Rep. 2020;10(1):10175. https://doi.org/10.1038/s41598-020-67138-8
41. Le RuEC, Etchegoin PG. Principles of surface-enhanced raman spectroscopy: and related plasmonic effects. 1st ed. Elsevier; 2009.
42. ICNIRP Guidelines on Limits of Exposure to Laser Radiation of Wavelengths between 180 nm and 1,000 μm. Health Phys. 2013;105(3):271–95. https://doi.org/10.1097/HP.0b013e3182983fd4
43. Jacques SL. Optical properties of biological tissues: a review. Phys Med Biol. 2013;58:R37–61. https://doi.org/10.1088/0031-9155/58/11/R37
44. Thomsen S. Pathologic analysis of photothermal and photomechanical effects of laser–tissue interactions. Photochem Photobiol. 1991;53(6):825–35. https://doi.org/10.1111/j.1751-1097.1991.tb09897.x
45. Bakker Schut TC, Witjes MJH, Sterenborg HJCM, Speelman OC, Roodenburg JLN, Marple ET, et al. In vivo detection of dysplastic tissue by Raman spectroscopy. Anal Chem. 2000;72(24):6010–8. https://doi.org/10.1021/ac000780u
46. Buschman HP, Marple ET, Wach ML, Bennett B, Bakker Schut TC, Bruining HA, et al. In vivo determination of the molecular composition of artery wall by intravascular Raman spectroscopy. Anal Chem. 2000;72(16):3771–5. https://doi.org/10.1021/ac000298b
47. Shim MG, Wong Kee Song LM, Marcon NE, Wilson BC. In vivo near-infrared Raman spectroscopy: demonstration of feasibility during clinical gastrointestinal endoscopy. Photochem Photobiol. 2000;72(1):146–50. https://doi.org/10.1562/0031-8655(2000)0720146IVNIRS2.0.CO2
48. Motz JT, Gandhi SJ, Scepanovic OR, Haka AS, Kramer JR, Dasari RR, et al. Real-time Raman system for in vivo disease diagnosis. J Biomed Opt. 2005;10(3):031113. https://doi.org/10.1117/1.1920247
49. Pilot R, Signorini R, Durante C, Orian L, Bhamidipati M, Fabris L. A review on surface-enhanced Raman scattering. Biosensors. 2019;9(2):57. https://doi.org/10.3390/bios9020057
50. Langer J, Jimenez de Aberasturi D, Aizpurua J, Alvarez-Puebla RA, Auguié B, Baumberg JJ, et al. Present and future of surface-

enhanced Raman scattering. ACS Nano. 2020;14(1):28–117. https://doi.org/10.1021/acsnano.9b04224

51. Pérez-Jiménez AI, Lyu D, Lu Z, Liu G, Ren B. Surface-enhanced Raman spectroscopy: benefits, trade-offs and future developments. Chem Sci. 2020;11(18):4563–77. https://doi.org/10.1039/d0sc00809e
52. Zong C, Xu M, Xu LJ, Wei T, Ma X, Zheng XS, et al. Surface-enhanced Raman spectroscopy for bioanalysis: reliability and challenges. Chem Rev. 2018;118(10):4946–80. https://doi.org/10.1021/acs.chemrev.7b00668
53. Zhang M, Li X, Pan J, Zhang Y, Zhang L, Wang C, et al. Ultrasensitive detection of SARS-CoV-2 spike protein in untreated saliva using SERS-based biosensor. Biosens Bioelectron. 2021;190: 113421. https://doi.org/10.1016/j.bios.2021.113421
54. Li X. Spectral analysis of human saliva for detection of lung cancer using surface-enhanced Raman spectroscopy. J Biomed Opt. 2012;17(3):037003. https://doi.org/10.1117/1.JBO.17.3.037003
55. Hernández-Arteaga A, de Jesús Zermeño Nava J, Kolosovas-Machuca ES, Velázquez-Salazar JJ, Vinogradova E, José-Yacamán M, et al. Diagnosis of breast cancer by analysis of sialic acid concentrations in human saliva by surface-enhanced Raman spectroscopy of silver nanoparticles. Nano Res. 2017;10(11):3662–70. https://doi.org/10.1007/s12274-017-1576-5
56. Lin X, Lin D, Ge X, Qiu S, Feng S, Chen R. Noninvasive detection of nasopharyngeal carcinoma based on saliva proteins using surface-enhanced Raman spectroscopy. J Biomed Opt. 2017;22(10):1. https://doi.org/10.1117/1.JBO.22.10.105004
57. Feng S, Huang S, Lin D, Chen G, Xu Y, Li Y, et al. Surface-enhanced Raman spectroscopy of saliva proteins for the noninvasive differentiation of benign and malignant breast tumors. Int J Nanomed. 2015;10:537–47. https://doi.org/10.2147/IJN.S71811
58. Li Xiaozhou, Yang Tianyue, Wang Rong, Wen Weidong. Surface enhanced Raman spectrum of saliva for detection of lung cancer. IEEE Int Symp IT Med Edu. 2011:688–90. https://doi.org/10.1109/ITiME.2011.6132093
59. Camacho SA, Sobral-Filho RG, Aoki PHB, Constantino CJL, Brolo AG. Zika immunoassay based on surface-enhanced Raman scattering nanoprobes. ACS Sens. 2018;3(3):587–94. https://doi.org/10.1021/acssensors.7b00639
60. Eom G, Hwang A, Kim H, Yang S, Lee DK, Song S, et al. Diagnosis of tamiflu-resistant influenza virus in human nasal fluid and saliva using surface-enhanced Raman scattering. ACS Sens. 2019;4(9):2282–7. https://doi.org/10.1021/acssensors.9b00697
61. Sebba D, Lastovich AG, Kuroda M, Fallows E, Johnson J, Ahouidi A, et al. A point-of-care diagnostic for differentiating ebola from endemic febrile diseases. Sci Transl Med. 2018;10(471): 1–12. https://doi.org/10.1126/scitranslmed.aat0944
62. Zhang Y, Tang Y, Hsieh YH, Hsu CY, Xi J, Lin KJ, et al. Towards a high-throughput label-free detection system combining localized-surface plasmon resonance and microfluidics. Lab Chip. 2012;12(17):3012. https://doi.org/10.1039/c2lc40590c
63. Žukovskaja O, Jahn I, Weber K, Cialla-May D, Popp J. Detection of *Pseudomonas aeruginosa* metabolite pyocyanin in water and saliva by employing the SERS technique. Sensors. 2017;17(8): 1704. https://doi.org/10.3390/s17081704
64. Hole A, Tyagi G, Deshmukh A, Deshpande R, Gota V, Chaturvedi P, et al. Salivary Raman spectroscopy: standardization of sampling protocols and stratification of healthy and oral cancer subjects. Appl Spectrosc. 2021;75(5):581–8. https://doi.org/10.1177/0003702820973260
65. Barranco A, Borras A, Gonzalez-Elipe AR, Palmero A. Perspectives on oblique angle deposition of thin films: from fundamentals to devices. Prog Mater Sci. 2016;76:59–153. https://doi.org/10.1016/j.pmatsci.2015.06.003
66. Suzuki M, Maekita W, Wada Y, Nagai K, Nakajima K, Kimura K, et al. Ag nanorod arrays tailored for surface-enhanced Raman imaging in the near-infrared region. Nanotechnology. 2008;19(26):265304. https://doi.org/10.1088/0957-4484/19/26/265304
67. Chaney SB, Shanmukh S, Dluhy RA, Zhao YP. Aligned silver nanorod arrays produce high sensitivity surface-enhanced Raman spectroscopy substrates. Appl Phys Lett. 2005;87(3):031908. https://doi.org/10.1063/1.1988980
68. Driskell JD, Shanmukh S, Liu Y, Chaney SB, Tang XJ, Zhao YP, et al. The use of aligned silver nanorod arrays prepared by oblique angle deposition as surface enhanced Raman scattering substrates. J Phys Chem C. 2008;112(4):895–901. https://doi.org/10.1021/jp075288u
69. Sheehy G, Picot F, Dallaire F, Ember K, Nguyen T, Petrecca K, et al. Open-sourced Raman spectroscopy data processing package implementing a baseline removal algorithm validated from multiple datasets acquired in human tissue and biofluids. J Biomed Opt. 2023;28:025002. https://doi.org/10.1117/1.JBO.28.2.025002
70. Dallaire F, Picot F, Tremblay JP, Sheehy G, Lemoine É, Agarwal R, et al. Quantitative spectral quality assessment technique validated using intraoperative in vivo Raman spectroscopy measurements. J Biomed Opt. 2020;25(04):1. https://doi.org/10.1117/1.jbo.25.4.040501
71. Le Ru EC, Blackie E, Meyer M, Etchegoin PG. Surface enhanced Raman scattering enhancement factors: A comprehensive study. J Phys Chem C. 2007;111(37):13794–803. https://doi.org/10.1021/jp0687908
72. Czamara K, Majzner K, Pacia MZ, Kochan K, Kaczor A, Baranska M. Raman spectroscopy of lipids: a review. J Raman Spectrosc. 2015;46(1):4–20. https://doi.org/10.1002/jrs.4607
73. Tiwari N. Study of adsorption behavior of aminothiophenols on gold nanorods using surface-enhanced Raman spectroscopy. J Nanophotonics. 2011;5(1):053513. https://doi.org/10.1117/1.3594096
74. Rygula A, Majzner K, Marzec KM, Kaczor A, Pilarczyk M, Baranska M. Raman spectroscopy of proteins: a review. J Raman Spectrosc. 2013;44(8):1061–76. https://doi.org/10.1002/jrs.4335
75. Talari ACS, Movasaghi Z, Rehman S, Rehman I. Raman spectroscopy of biological tissues. Appl Spectrosc Rev. 2015;50(1):46–111. https://doi.org/10.1080/05704928.2014.923902
76. Pegoraro AF, Ridsdale A, Moffatt DJ, Jia Y, Pezacki JP, Stolow A. Optimally chirped multimodal CARS microscopy based on a single Ti:sapphire oscillator. Opt Express. 2009;17(4):2984. https://doi.org/10.1364/OE.17.002984
77. Di Napoli C, Pope I, Masia F, Watson P, Langbein W, Borri P. Hyperspectral and differential CARS microscopy for quantitative chemical imaging in human adipocytes. Biomed Opt Express. 2014;5(5):1378. https://doi.org/10.1364/BOE.5.001378
78. Camp Jr. CH, Lee YJ, Heddleston JM. High-speed coherent Raman fingerprint imaging of biological tissues. Nat Photonics. 2014;8(8):627–34. https://doi.org/10.1038/nphoton.2014.145

SUPPORTING INFORMATION

Additional supporting information can be found online in the Supporting Information section at the end of this article.

How to cite this article: Zamani E, Ksantini N, Sheehy G, Ember KJI, Baloukas B, Zabeida O, et al. Spectral effects and enhancement quantification in healthy human saliva with surface-enhanced Raman spectroscopy using silver nanopillar substrates. Lasers Surg Med. 2024;56:206–217. https://doi.org/10.1002/lsm.23746